

# One-Dimensional Transport of Bosons between Weakly Linked Reservoirs

D. P. Simpson,<sup>1</sup> D. M. Gangardt,<sup>1</sup> I. V. Lerner,<sup>1</sup> and P. Krüger<sup>2</sup>

<sup>1</sup>*School of Physics and Astronomy, University of Birmingham, Edgbaston, Birmingham, B15 2TT, United Kingdom*

<sup>2</sup>*Midlands Ultracold Atom Research Centre, School of Physics and Astronomy, University of Nottingham, University Park, Nottingham, NG7 2RD, UK*

(Dated: 7 January 2014; revised 13 February 2014)

We study a flow of ultracold bosonic atoms through a one-dimensional channel that connects two macroscopic three-dimensional reservoirs of Bose-condensed atoms via weak links implemented as potential barriers between each of the reservoirs and the channel. We consider reservoirs at equal chemical potentials so that a superflow of the quasi-condensate through the channel is driven purely by a phase difference,  $2\Phi$ , imprinted between the reservoirs. We find that the superflow never has the standard Josephson form  $\sim \sin 2\Phi$ . Instead, the superflow discontinuously flips direction at  $2\Phi = \pm\pi$  and has metastable branches. We show that these features are robust and not smeared by fluctuations or phase slips. We describe a possible experimental setup for observing these phenomena.

PACS numbers: 74.55.+v, 03.75.Lm, 05.60.Gg

Recent advances in trapping and manipulating ultracold gases have enabled experimental observations of a variety of new transport phenomena in quasi-one-dimensional (1D) cold atom systems [1–7], complementary to those extensively studied in condensed matter physics. Correlation effects play a crucial role in the behavior of 1D systems and a lot of theoretical effort has been concentrated on the understanding of such effects in ultracold gases (see for reviews [8, 9]).

In particular, correlation effects are responsible for a drastic modification of tunneling into a 1D channel and of a 1D flow across a single imperfection, impurity or weak link, as has been shown in numerous theoretical [10–13] and experimental [14–17] studies of electronic transport in systems such as semiconductor quantum wires or carbon nanotubes. A geometry where these types of phenomena can be observed for ultracold atomic systems has rapidly attracted theoretical interest [18–20] and has been recently realized experimentally [4, 5] by connecting 3D fermionic reservoirs via a 1D channel. A similar experiment with ultracold *bosons* would lead to the intriguing opportunity to explore coherent 1D transport fo-

cus on features without a direct analogy in condensed matter systems.

In this Letter we study a 1D flow of degenerate ultracold bosons driven by a phase difference between two macroscopic Bose–Einstein condensates (BEC), which are weakly connected by a 1D channel via two tunneling barriers (see Fig 1).

We demonstrate that the bosonic flow behaves drastically different to its condensed matter counterpart, i.e., an electronic flow between two bulk superconductors weakly connected by a 1D channel via Josephson junctions [21, 22]. We show that qualitatively new physics emerges here. The external phase difference between the reservoirs governs the phase profile illustrated in Fig. 2: substantial phase drops at the tunneling barriers are followed by a constant superflow of the quasicondensate through the 1D channel. Such a superflow is parametrically larger than that expected from a perturbative approach, which is appropriate for the corresponding electronic case [21] but totally fails for the bosonic superflow. Surprisingly, for an external phase difference close to  $\pi$ , the phase profile turns out to be always bistable so that the superflow can spontaneously change direction (see Fig. 3). With increasing the tunneling, such a bistability spreads to all values of  $\Phi$ . This would lead to jumps and hysteresis in the sawtoothlike observable superflow, making it qualitatively different from an almost sinusoidal Josephson supercurrent in the corresponding superconducting systems.

The geometry sketched in Fig. 1, required for observing these phenomena in flows of ultracold bosons, can be experimentally implemented by exploiting the versatility of potential shaping on atom chips [23]. Here we can form two bulk reservoirs weakly connected by a 1D channel and imprint an arbitrary phase difference between them, while keeping the chemical potentials equal [24].

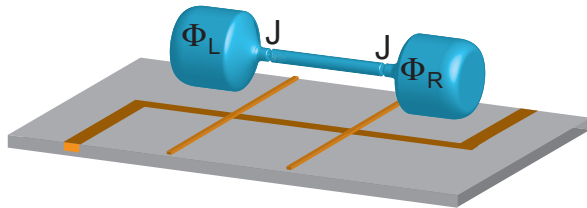


FIG. 1. (Color online) A sketch of two 3D BEC reservoirs connected by a 1D channel via weak tunneling links. A simplified illustration of an atom chip creating an appropriate magnetic trapping configuration is also shown.

This scenario is a starting point for experimental studies of different regimes of the bosonic superflow that we investigate theoretically in this Letter. We will show how the results described above are obtained from a mean-field approach and prove it to be robust against fluctuations.

We consider a system comprising two bulk reservoirs, each containing a BEC, which are coupled via a 1D channel separated from the reservoirs by weak tunnelling barriers, see Fig. 1. The BEC in the left and right reservoirs is described by order parameters  $\Psi_{L,R} = \sqrt{N_{L,R}}e^{i\Phi_{L,R}}$ . Without loss of generality, we choose  $\Phi_L = -\Phi_R \equiv \Phi$ . We assume that the reservoirs have been equilibrated to the same chemical potential and thus have equal particle densities,  $n_L = n_R$ , so that the current through the channel is driven only by the phase difference  $2\Phi$ .

The  $N$  bosons in a 1D channel of length  $L$  form a quasicondensate described by an order parameter  $\psi(x, t) = \sqrt{n + \rho(x, t)}e^{i\varphi(x, t)}$ , where  $\varphi$  is a phase field and  $\rho$  denotes density fluctuations around the mean density  $n = N/L$ . As  $\rho$  and  $\varphi$  are canonically conjugate, the imaginary-time action describing phononlike low-energy excitations can be written via  $\varphi$  alone and, assuming that  $L \gg \xi$ , has the standard Luttinger-liquid form [25]:

$$S_{LL} = \frac{K}{2\pi c} \int_0^\beta d\tau \int_{-L/2}^{L/2} dx [(\partial_\tau \varphi)^2 + c^2(\partial_x \varphi)^2]. \quad (1)$$

Here  $\xi \equiv 1/mc$  is the healing length [26],  $c$  is the sound velocity,  $m$  is the bosonic mass,  $K \equiv \pi n \xi$  is the Luttinger parameter:  $K \geq 1$  for bosons with a short-range repulsion, with  $K = 1$  corresponding to the Tonks-Girardeau gas of hard-core bosons equivalent to the ideal Fermi gas [25]. For typical experimental situations,  $\xi$  is much larger than the distance between bosons, so that  $K \gg 1$ .

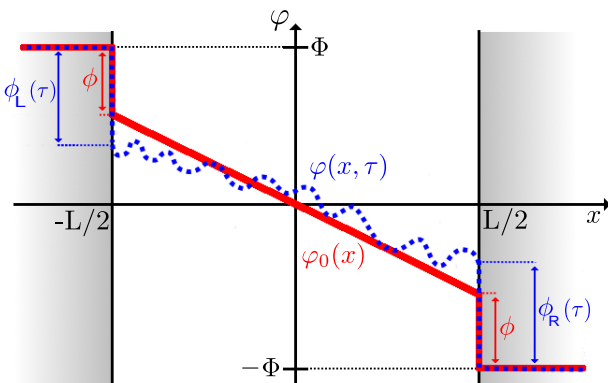


FIG. 2. (Color online) Phase profile along the channel. The solid line,  $\varphi_0(x)$  is a typical (symmetric) configuration made up of a linear superfluid contribution and phase jumps,  $\phi$ , at each tunnel barrier. The dashed line represents a fluctuation around the phase profile. Here we have chosen the phases of the BEC reservoirs as  $\Phi_L = -\Phi_R \equiv \Phi$ . The phase profile shown above corresponds to a phase difference of  $2\Phi < \pi$ .

We model the coupling of the reservoirs to the channel by a tunneling action, assuming for simplicity[27] the tunneling energies at both barriers being equal to  $J$ :

$$S_T = 2J \int_0^\beta d\tau [\cos \phi_R + \cos \phi_L], \quad (2)$$

where  $\phi_{L,R}$  are the expected phase drops at the barriers ( $x = \pm L/2$ ). As usual, the tunneling action is valid when the overlap of the wave functions across the barrier is small, which imposes the requirement  $J \ll cK/\xi \equiv \pi nc$ .

A second order in  $J$  perturbational calculation of the bosonic supercurrent gives a result divergent at  $T \rightarrow 0$  for the values of  $K$  pertinent to bosonic systems. So, unlike superconducting systems [21], for which the perturbative approach is fully adequate, a nonperturbative treatment is required here.

We start our analysis with finding a nontrivial mean-field (MF) configuration for the model (1) and (2). The phase field  $\varphi(x)$  in the channel is related to the phase drops at the barriers by the boundary conditions:

$$\phi_L = \Phi - \varphi(-L/2), \quad \phi_R = \Phi + \varphi(L/2). \quad (3)$$

Then we minimize the action (1)–(2) by a stationary solution satisfying the above boundary condition:

$$\varphi_0(x) = -\phi_- - 2(\Phi - \phi_+) \frac{x}{L}, \quad \phi_\pm \equiv \frac{1}{2}(\phi_L \pm \phi_R). \quad (4)$$

It describes a constant superflow,  $\mathcal{I} = nv$ , between the reservoirs, with a velocity  $v = -2(\Phi - \phi_+)/mL$ . The energy  $E$  is the sum of the supercurrent kinetic energy,  $\frac{1}{2}mNv^2$ , which arises from the Luttinger action Eq. (1) on substituting ansatz (4), and the Josephson energy,  $-2J(\cos \phi_R + \cos \phi_L)$ . The total dimensionless energy,  $\varepsilon \equiv E/J_c$ , can be written via the phase drops  $\phi_\pm$  as

$$\varepsilon = 2(\Phi - \phi_+)^2 - 4\alpha \cos \phi_+ \cos \phi_-, \quad \alpha \equiv J/J_c \quad (5)$$

where  $J_c \equiv n/mL \ll \pi nc$  so that  $\alpha$  can vary from 0 to values  $\gg 1$  within the region of applicability of the tunneling Hamiltonian, Eq. (2).

All possible MF solutions are obtained by minimizing  $\varepsilon$  with respect to  $\phi_+$  and  $\phi_-$  at a fixed  $\Phi$  which gives

$$\Phi - \phi_+ = \alpha \sin \phi_+ \cos \phi_-, \quad (6a)$$

$$\cos \phi_+ \sin \phi_- = 0. \quad (6b)$$

Since energy (5) is a  $2\pi$  periodic function of  $\phi_-$ , we can restrict ourselves to two solutions of Eq. (6b), corresponding to the symmetric phase drops,  $\phi_- = 0$  so that  $\phi_R = \phi_L = \phi_+$ , and asymmetric ones,  $\phi_- = \pi$  so that  $\phi_L = \phi_+ + \pi$ . Solutions corresponding to  $\cos \phi_+ = 0$  are always unstable (saddle points). For the symmetric/asymmetric branch Eq. (6a) is reduced to

$$\Phi - \phi_+ = \pm \alpha \sin \phi_+ \quad (6c)$$

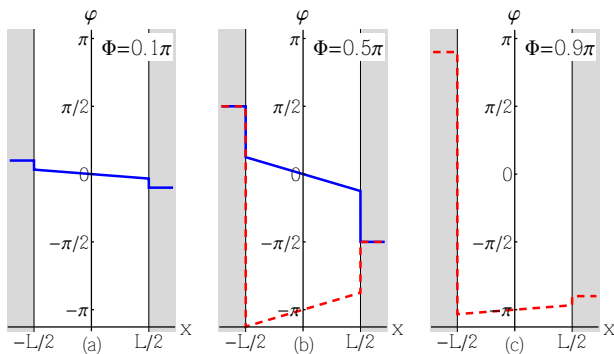


FIG. 3. (Color online) The MF phase profile in the channel for  $\alpha < 1$  ( $J < J_c$ ): (a) and (c) are unique symmetric/asymmetric solutions near  $\Phi = 0$  or  $\pi$ , respectively; (b) these two solutions become degenerate at  $\Phi = \pi/2$ , with one of them becoming metastable slightly above or below  $\pi/2$ .

The symmetric-branch equation is almost identical to that emerging in a text-book analysis of a superconducting quantum interference device (SQUID) [28]; however, its solution has a peculiar  $4\pi$  periodicity. It is the coexistence of this solution with that for the asymmetric branch which restores the correct  $2\pi$  periodicity. Indeed, each of Eqs. (6c) has at least one stable solution in some interval of  $\Phi$  and, remarkably, these intervals always overlap.

The MF energy is thus no longer a single-valued function of  $\Phi$ . Assuming first a singly connected geometry, when the external phase difference  $2\Phi \in [0, 2\pi]$ , we find for small  $\Phi$  that the lowest energy solution of Eq. (6a), which is  $\phi_+ \approx \Phi/(1 + \alpha)$ , belongs to the symmetric branch. An elementary analysis shows that for small  $\alpha$  it remains stable with increasing  $\Phi$  up to  $\Phi = \pi/2 + \alpha$ . The lowest-energy solution around  $\Phi = \pi$  belongs to the asymmetric branch and remains stable down to  $\Phi = \pi/2 - \alpha$ . Thus, in the interval of width  $2\alpha$  centered at  $\Phi = \pi/2$  the two solutions coexist: the symmetric solution is stable and the asymmetric is metastable at  $\Phi < \pi/2$ , with their roles reversing at  $\Phi > \pi/2$ , as illustrated in Fig. 3.

With  $\alpha$  increasing, two new solutions appear at  $\alpha > 1$  for both the symmetric and asymmetric branch but they remain unstable until  $\alpha$  reaches  $\pi/2$ . At this point the two solutions coexist in the entire interval  $[0, \pi]$ , while new metastable solutions emerge for the asymmetric branch around  $\Phi = 0$  and for the symmetric around  $\Phi = \pi$ . With  $\alpha$  further increasing, new pairs of metastable solutions appear at integer multiples of  $\pi/2$ , see Fig. 4.

It follows from Eqs. (4) and (6a) that the superflow along the channel is  $\mathcal{I} = \mp 2J \sin \phi_+$ . As the sign comes from  $\cos \phi_- = \pm 1$ , it is easy to see that this corresponds to the sum of the Josephson currents across the barriers,  $-J(\sin \phi_L + \sin \phi_R)$ , as expected. What is non-trivial is the relation of this to the external phase difference,  $2\Phi$ ,

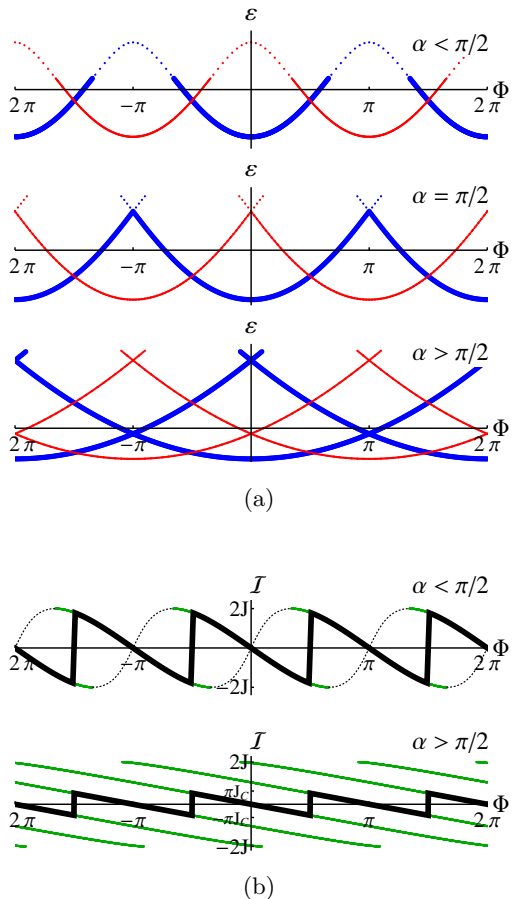


FIG. 4. (Color online) (a) The MF energies (5), spread between  $\varepsilon_{\min} = -4\alpha$  and  $\varepsilon_{\max} = 2\alpha^2$ , as functions of the external phase difference,  $2\Phi$ , at different values of  $\alpha$ . Thick (thin) solid lines represent symmetric (asymmetric) stable or metastable solutions, the latter lying in the continuum of phononic excitations. (b) The dependence of the superflow on  $2\Phi$ , with thick (thin) lines representing stable (metastable) flow. Dashed lines represent unstable solutions drawn as a guide to the eye.

given by Eqs. (6).

For small  $\alpha$  (i.e. for  $J \ll J_c$ ),  $\phi_+ \approx \Phi \mp \alpha \sin \Phi$  so that almost the entire phase change accumulates at the Josephson barriers. The phase drops look very different for the two branches, symmetric with  $\phi_- = 0$  and asymmetric with  $\phi_- = \pi$ . In the former case,  $\phi_L = \phi_R$  by definition while in the latter  $\phi_L = \Phi + \pi$  and  $\phi_R = \Phi - \pi$ . This means that, e.g., near the energy minimum  $\Phi = \pi$ , almost the entire phase drop,  $2\pi$ , occurs at one of the barriers. The phase profiles described by these two branches correspond to the superflows  $\mp 2J \sin \Phi$ , each being  $4\pi$  periodic with respect to the overall phase difference  $2\Phi$ . As the symmetric branch is stable for  $2\Phi < \pi + 2\alpha$  and asymmetric for  $2\Phi > \pi - 2\alpha$ , the correct  $2\pi$  periodicity is restored by jumps between the branches which can occur anywhere in the intervals of coexistence.

With  $\alpha$  increasing, the metastable energy solutions are

reflected in the superflow,  $\mathcal{I} = -J_c d\varepsilon/d(2\Phi)$ , Fig. 4(b). The superflow corresponding to the lowest energy configuration changes from the piecewise sinusoid for  $\alpha < \pi/2$  to a sawtooth function at  $\alpha > \pi/2$ , given by  $\mathcal{I} = -2J_c\Phi$  for  $\Phi \in [-\pi/2, \pi/2]$  and periodically repeated for all  $\Phi$ . In the latter case, when  $J \gg J_c$ , the maximal possible superflow saturates at  $\mathcal{I} = \pi J_c$ . Such a characteristic sawtooth shape for any value of the tunneling is an inevitable consequence of the metastability. In contrast, for the case of superconductors connected by a LL channel via two JJ (corresponding in our notations to  $K < 1/2$ ), the perturbative Josephson current has a slightly distorted sinusoidal shape [21]. It is interesting that the exact solution for the boundary case,  $K = 1/2$ , shows a crossover from a smooth to a saw-tooth shape with increasing the tunneling [22].

The existence of metastable solutions should reveal itself experimentally in hysteresis of the superflow, as we will discuss at the end of the Letter.

It is important that phonon fluctuations in the channel do not wash out essential features of the MF solutions, Eqs. (4)–(6), and remarkable that they do not result in avoided crossings in Fig. 4(a). To show this we introduce the phase fluctuations in the 1D channel,  $\tilde{\varphi}(x, \tau) = \varphi(x, \tau) - \varphi_0(x)$  and at the boundaries,  $\tilde{\phi}_{L,R}(\tau) = \phi_{L,R}(\tau) - \phi_{L,R}$ , related by the boundary conditions  $\tilde{\varphi}(\pm L/2, \tau) = \pm \tilde{\phi}_{L,R}(\tau)$ . Here  $\varphi_0(x)$  and  $\phi_{L,R}$  are the solutions of the MF equations (6) described above, related to the symmetric and antisymmetric combinations introduced in Eq. (4). Then, after integrating out the Gaussian fluctuations in the 1D channel, we obtain the effective action,  $S = S_{\text{fl}} + S_\varepsilon$ :

$$S_{\text{fl}} = K \int \frac{|\omega| d\omega}{2\pi^2} \left[ |\tilde{\phi}_+(\omega)|^2 + |\tilde{\phi}_-(\omega)|^2 \right], \quad (7a)$$

$$S_\varepsilon = \int d\tau \varepsilon[\phi_+(\tau), \phi_-(\tau); \Phi]. \quad (7b)$$

Here  $\varepsilon$  is the function of  $\phi_\pm(\tau) = \tilde{\phi}_\pm(\tau) + \phi_\pm$  and is given by Eq. (5). It plays the role of an effective ‘‘washboard’’ potential for the Caldeira-Legget type action of Eq. (7a). We assumed in deriving Eq. (7a) that  $\omega \gg \pi c/L$ , which is the lowest phonon energy in the channel [24].

Now we perform the standard renormalization group (RG) analysis by integrating out fast modes in the fields  $\phi_+$  and  $\phi_-$ , as described for completeness in Supplemental Material [24]. This results in the RG equation for the dimensionless tunneling strength  $\alpha$ :

$$\frac{d \ln \alpha}{d \ln b} = 1 - \frac{1}{2K}, \quad (8)$$

where  $b$  is a scaling parameter. The integration between the upper,  $\Lambda \sim c/\xi$ , and lower,  $\omega_0 \sim \max\{T, c/L\}$ , energy cutoffs gives the renormalized dimensionless tunneling as  $\alpha(\omega_0) = \alpha_0 (\Lambda/\omega_0)^{1 - \frac{1}{2K}}$ , where  $\alpha_0 \equiv J/J_c$ . Since the tunneling through barriers separated by  $L \gg \xi$  is

uncorrelated, this is similar to the results for tunneling through a single barrier [10], as well as to the results for superconducting systems [21] in a geometry similar to that under consideration here.

A remarkable feature is that for  $K \gg 1$ , characteristic of ultracold bosonic systems with the healing length much bigger than the interatomic distance,  $\alpha$  flows to larger values. This means that the washboard potential becomes more pronounced so that the fluctuations are irrelevant in the low-energy limit and the MF solution, described above, is robust. In particular, since the fluctuations do not connect different MF branches, the level crossings are not avoided and the characteristic cusps in energy, Fig. 4, and the corresponding jumps in the superflow remain. Alternatively, this can be seen using instanton techniques similar to those of Ref. [29]. Namely, the probability of an instanton connecting two degenerate configurations, like in Fig. 3(b), can be shown to be vanishingly small for  $K \gg 1$ .

Experimental data about the superflow can be extracted from images taken of the atomic density distribution in the channel at different times throughout the evolution of the system. The phase imprinting can be implemented in two different ways. First, we can imprint the phase difference before connecting the reservoirs thus mapping the lowest, stable branches of the energy (Fig. 4), and measuring jumps in the superflow direction. Secondly, we can gradually modify the phase difference *in vivo*, with the weak link already present, thus being able to explore the metastable branches by observing a hysteretic behavior in the superflow.

Complementary direct measurements of the phase profile are possible by keeping part of the bulk BEC as a homogenous phase reference. Then a readout can be obtained from an interference pattern between this reference and the quasicondensate in the channel [24].

In conclusion, we have demonstrated that bosonic superflow driven by a phase difference between two BEC reservoirs has spectacular features without any analogy in geometrically similar superconducting systems. The superflow, which is proportional to the first (rather than second) power of the tunneling energy, periodically flips direction and, moreover, has metastable branches, Fig. 4. The corresponding energy levels intersect, and fluctuations do not lead to avoided crossings. The bi- and multistability associated with the existence of metastable branches can only be accessed dynamically. A theoretical description of the kinetics of such a process, while going beyond the scope of this Letter, remains an interesting open question. Experimentally, the multistability can be revealed by gradually adjusting the phase difference between the reservoirs at finite tunneling.

We gratefully acknowledge support from the Leverhulme Trust via the Grant No. RPG-380 (I.V.L.) and from the EPSRC.

- 
- [1] J. Billy, V. Josse, Z. Zuo, A. Bernard, B. Hambrecht, P. Lukan, D. Clement, L. Sanchez-Palencia, P. Bouyer, and A. Aspect, *Nature* **453**, 891 (2008); G. Roati, C. D'Errico, L. Fallani, M. Fattori, C. Fort, M. Zaccanti, G. Modugno, M. Modugno, and M. Inguscio, *ibid.* **453**, 895 (2008).
- [2] S. Levy, E. Lahoud, I. Shomroni, and J. Steinhauer, *Nature* **449**, 579 (2007).
- [3] S. Palzer, C. Zipkes, C. Sias, and M. Köhl, *Phys. Rev. Lett.* **103**, 150601 (2009); J. Catani, G. Lamporesi, D. Naik, M. Gring, M. Inguscio, F. Minardi, A. Kantian, and T. Giamarchi, *Phys. Rev. A* **85**, 023623 (2012).
- [4] J.-P. Brantut, J. Meineke, D. Stadler, S. Krinner, and T. Esslinger, *Science* **337**, 1069 (2012).
- [5] D. Stadler, S. Krinner, J. Meineke, J.-P. Brantut, and T. Esslinger, *Nature* **491**, 736 (2012).
- [6] A. Ramanathan, K. C. Wright, S. R. Muniz, M. Zelan, W. T. Hill, C. J. Lobb, K. Helmerson, W. D. Phillips, and G. K. Campbell, *Phys. Rev. Lett.* **106**, 130401 (2011).
- [7] L. Tanzi, E. Lucioni, S. Chaudhuri, L. Gori, A. Kumar, C. D'Errico, M. Inguscio, and G. Modugno, *Phys. Rev. Lett.* **111**, 115301 (2013).
- [8] M. A. Cazalilla, R. Citro, T. Giamarchi, E. Orignac, and M. Rigol, *Rev. Mod. Phys.* **83**, 1405 (2011).
- [9] A. Imambekov, T. L. Schmidt, and L. I. Glazman, *Rev. Mod. Phys.* **84**, 1253 (2012).
- [10] C. L. Kane and M. P. A. Fisher, *Phys. Rev. Lett.* **68**, 1220 (1992); *Phys. Rev. B* **46**, 15233 (1992).
- [11] K. A. Matveev, D. Yue, and L. I. Glazman, *Phys. Rev. Lett.* **71**, 3351 (1993); A. Furusaki and N. Nagaosa, *Phys. Rev. B* **47**, 4631 (1993); M. Fabrizio and A. O. Gogolin, *Phys. Rev. B* **51**, 17827 (1995).
- [12] A. Furusaki and K. A. Matveev, *Phys. Rev. Lett.* **88**, 226404 (2002); Y. V. Nazarov and L. I. Glazman, **91**, 126804 (2003); D. G. Polyakov and I. V. Gornyi, *Phys. Rev. B* **68**, 035421 (2003).
- [13] I. V. Lerner, V. I. Yudson, and I. V. Yurkevich, *Phys. Rev. Lett.* **100**, 256805 (2008); M. Goldstein and R. Berkovits, *Phys. Rev. Lett.* **104**, 106403 (2010).
- [14] M. Bockrath, D. H. Cobden, J. Lu, A. G. Rinzler, R. E. Smalley, L. Balents, and P. L. McEuen, *Nature* **397**, 598 (1999); M. Bockrath, W. J. Liang, D. Bozovic, J. H. Hafner, C. M. Lieber, M. Tinkham, and H. K. Park, *Science* **291**, 283 (2001).
- [15] Z. Yao, H. W. C. Postma, L. Balents, and C. Dekker, *Nature* **402**, 273 (1999).
- [16] O. M. Auslaender, A. Yacoby, R. de Picciotto, K. W. Baldwin, L. N. Pfeiffer, and K. W. West, *Science* **295**, 825 (2002); L. Venkataraman, Y. S. Hong, and P. Kim, *Phys. Rev. Lett.* **96**, 076601 (2006).
- [17] E. Levy, A. Tsukernik, M. Karpovski, A. Palevski, B. Dwir, E. Pelucchi, A. Rudra, E. Kapon, and Y. Oreg, *Phys. Rev. Lett.* **97**, 196802 (2006); E. Levy, I. Sternfeld, M. Eshkol, M. Karpovski, B. Dwir, A. Rudra, E. Kapon, Y. Oreg, and A. Palevski, *Phys. Rev. B* **85**, 045315 (2012).
- [18] T. Paul, M. Hartung, K. Richter, and P. Schlagheck, *Phys. Rev. A* **76**, 063605 (2007).
- [19] D. B. Gutman, Y. Gefen, and A. D. Mirlin, *Phys. Rev. B* **85**, 125102 (2012).
- [20] L. H. Kristinsdóttir, O. Karlström, J. Bjerlin, J. C. Cremon, P. Schlagheck, A. Wacker, and S. M. Reimann, *Phys. Rev. Lett.* **110**, 085303 (2013).
- [21] R. Fazio, F. W. J. Hekking, and A. A. Odintsov, *Phys. Rev. Lett.* **74**, 1843 (1995); *Phys. Rev. B* **53**, 6653 (1996); D. L. Maslov, M. Stone, P. M. Goldbart, and D. Loss, *Phys. Rev. B* **53**, 1548 (1996); I. Affleck, J.-S. Caux, and A. M. Zagoskin, *Phys. Rev. B* **62**, 1433 (2000).
- [22] J.-S. Caux, H. Saleur, and F. Siano, *Phys. Rev. Lett.* **88**, 106402 (2002); *Nucl. Phys. B* **672**, 411 (2003).
- [23] R. Folman, P. Krüger, D. Cassettari, B. Hessmo, T. Maier, and J. Schmiedmayer, *Phys. Rev. Lett.* **84**, 4749 (2000); R. Folman, P. Krüger, J. Schmiedmayer, J. Denschlag, and C. Henkel, *Advances In Atomic, Molecular, and Optical Physics*, **48**, 263356 (2002).
- [24] See *Supplemental Online Materials* for detail.
- [25] T. Giamarchi, *Quantum Physics in One Dimension* (Clarendon Press, London, 2004); A. O. Gogolin, A. A. Nersisyan, and A. M. Tsvelik, *Bosonization and Strongly Correlated Systems* (Cambridge University Press, Cambridge, 2004).
- [26] Here and elsewhere in the Letter we use units with  $\hbar = 1$ .
- [27] Allowing for a difference in the tunneling energies at both barriers leads insignificant changes in parameters without qualitatively affecting our results [24].
- [28] M. Tinkham, *Introduction to Superconductivity* (Dover, New York, 1996) p.226.
- [29] H. P. Büchler, V. B. Geshkenbein, and G. Blatter, *Phys. Rev. Lett.* **87**, 100403 (2001); M. Schechter, A. Kamenev, D. M. Gangardt, and A. Lamacraft, *Phys. Rev. Lett.* **108**, 207001 (2012).

## SUPPLEMENTAL ONLINE MATERIAL

### Fluctuational Action

We consider fluctuations around the mean field (MF) solution,  $\varphi_0(x)$ , given by Eqs. (4)-(6) of the main text. The fluctuations in the one dimensional (1D) channel are defined as  $\tilde{\varphi}(x, \tau) = \varphi(x, \tau) - \varphi_0(x)$  and the independent fluctuations at the boundaries are  $\tilde{\phi}_{L,R}(\tau) = \phi_{L,R}(\tau) - \phi_{L,R}$ . These fluctuations must obey the same boundary conditions as the MF solution so that  $\tilde{\varphi}(-L/2, \tau) = -\tilde{\phi}_L(\tau)$  and  $\tilde{\varphi}(L/2, \tau) = \tilde{\phi}_R(\tau)$ . It is convenient for what follows to introduce the field combinations  $2\tilde{\phi}_{\pm}(\tau) = \tilde{\phi}_L(\tau) \pm \tilde{\phi}_R(\tau)$ , as in Eq. (4) of the main text.

It is simple to see that the tunneling action, Eq. (2), is given in terms of these fluctuations as:

$$S_J = 2J \int d\tau [\cos \phi_L(\tau) + \cos \phi_R(\tau)] = 4J \int d\tau \cos(\phi_+ + \tilde{\phi}_+(\tau)) \cos(\phi_- + \tilde{\phi}_-(\tau)). \quad (9)$$

We now consider the fluctuations in the 1D channel. After taking into account the boundary conditions, the phase field in the 1D channel is  $\varphi(x, \tau) = -\phi_-(\tau) - \frac{2x}{L}(\Phi - \phi_+(\tau)) + \sum_{n=1}^{\infty} \left[ \varphi_n^e(\tau) \cos \frac{(2n-1)\pi x}{L} + \varphi_n^o(\tau) \sin \frac{2\pi n x}{L} \right]$ . Here the first two terms are the fluctuating counterparts of the MF solution while the remainder, which satisfies the Dirichlet boundary conditions at  $x = \pm L/2$ , is Fourier expanded. Substituting this into the Luttinger action (1) and performing the Fourier transform in  $\tau$  gives  $S = S_\varepsilon + S_0 + S_o + S_e$ , where

$$S_\varepsilon = \int d\tau \left[ 2J_c(\Phi - \phi_+)^2 - 4J_c(\Phi - \phi_+) \tilde{\phi}_+(\tau) + 4J \cos(\phi_+ + \tilde{\phi}_+(\tau)) \cos(\phi_- + \tilde{\phi}_-(\tau)) \right] \quad (10)$$

and

$$\begin{aligned} S_0 &= \frac{Kc}{2\pi} \int \frac{d\omega}{2\pi} \left[ \left( \frac{4}{L} + \frac{L\omega^2}{3c^2} \right) |\tilde{\phi}_+(\omega)|^2 + \frac{L\omega^2}{c^2} |\tilde{\phi}_-(\omega)|^2 \right] \\ S_o &= \frac{Kc}{2\pi} \int \frac{d\omega}{2\pi} \sum_{n=1}^{\infty} \left[ \frac{1}{2} \left( \frac{4\pi^2 n^2}{L} + \frac{L\omega^2}{c^2} \right) |\varphi_n^o(\omega)|^2 - \frac{2L(-1)^n \omega^2}{n\pi c^2} \tilde{\phi}_+(\omega) \varphi_n^o(-\omega) \right] \\ S_e &= \frac{Kc}{2\pi} \int \frac{d\omega}{2\pi} \sum_{n=1}^{\infty} \left[ \frac{1}{2} \left( \frac{(2n-1)^2 \pi^2}{L} + \frac{L\omega^2}{c^2} \right) |\varphi_n^e(\omega)|^2 + \frac{4L(-1)^n \omega^2}{\pi(2n-1)c^2} \tilde{\phi}_-(\omega) \varphi_n^e(-\omega) \right]. \end{aligned} \quad (11)$$

The only non-Gaussian part of the action, Eq. (10), does not depend on the fields in the channel,  $\varphi^e$  and  $\varphi^o$ , so that they can be integrated out. By symmetry, the even and odd parts of the fluctuational field,  $\varphi^e$  and  $\varphi^o$ , are not mixed and can be integrated out independently. Integrating out the odd fluctuations gives

$$\begin{aligned} \int \mathcal{D}\varphi_n^o e^{-S_o[\varphi_n^o]} &= \exp \left[ \frac{K}{2\pi c} \int \frac{d\omega}{2\pi} \sum_{n=1}^{\infty} \frac{2L^3 \omega^4 |\tilde{\phi}_+(\omega)|^2}{n^2 \pi^2 (4\pi^2 n^2 c^2 + L^2 \omega^2)} \right] \\ &= \exp \left[ -\frac{K}{2\pi} \int \frac{d\omega}{2\pi} |\tilde{\phi}_+(\omega)|^2 \left( 2\omega \coth \left( \frac{\omega L}{2c} \right) - \frac{4c}{L} - \frac{\omega^2 L}{3c} \right) \right]. \end{aligned} \quad (12)$$

Similarly, integrating out the even fluctuations gives

$$\begin{aligned} \int \mathcal{D}\varphi_n^e e^{-S_e[\varphi_n^e]} &= \exp \left[ \frac{K}{2\pi c} \int \frac{d\omega}{2\pi} \sum_{n=1}^{\infty} \frac{8L^3 \omega^4 |\tilde{\phi}_-(\omega)|^2}{(2n-1)^2 \pi^2 [(2n-1)^2 \pi^2 c^2 + L^2 \omega^2]} \right] \\ &= \exp \left[ -\frac{K}{2\pi} \int \frac{d\omega}{2\pi} |\tilde{\phi}_-(\omega)|^2 \left( 2\omega \tanh \left( \frac{\omega L}{2c} \right) - \frac{\omega^2 L}{c} \right) \right]. \end{aligned} \quad (13)$$

Combining Eqs. (12) and (13) with action  $S_0$ , i.e. the first line of Eq. (11), gives the full fluctuational action in terms of the fluctuating boundary fields:

$$S_{\text{fl}} = \int \frac{d\omega}{2\pi} \frac{K\omega}{\pi} \left[ \coth \left( \frac{\omega L}{2c} \right) |\tilde{\phi}_+(\omega)|^2 + \tanh \left( \frac{\omega L}{2c} \right) |\tilde{\phi}_-(\omega)|^2 \right] \quad (14)$$

This action can be further simplified at relevant energies,  $\omega \gg c/L \equiv \omega_0$  which is the lowest phononic energy in the system. The fluctuational action is then

$$S_{\text{fl}} = \frac{K}{\pi} \int \frac{d\omega}{2\pi} |\omega| \left[ |\tilde{\phi}_+(\omega)|^2 + |\tilde{\phi}_-(\omega)|^2 \right] \equiv \frac{K}{2\pi} \int \frac{d\omega}{2\pi} |\omega| \left[ |\tilde{\phi}_L(\omega)|^2 + |\tilde{\phi}_R(\omega)|^2 \right]. \quad (15)$$

in accordance with Eq. (7a) of the main text. The full action (7) will be used for an RG analysis with  $\omega_0$  playing the role of the infrared cutoff and  $\mu \equiv c/\xi$  the ultraviolet cutoff.

### RG Analysis

We perform the standard renormalization group (RG) analysis of the fluctuational action Eq. (7), which is equal to the sum of actions (10) and (15). It is convenient to do this in terms of the original fields  $\phi_{L,R}(\tau) = \phi_+(\tau) \pm \phi_-(\tau)$ , describing phase drops on the left and right barrier. To this end, we split the fields into the fast and slow modes,  $\phi_{L,R}(\tau) = \phi_{L,R}^>(\tau) + \phi_{L,R}^<(\tau)$ , comprising the Fourier components with energies  $\Lambda/b < |\omega| < \Lambda$  and  $|\omega| < \Lambda/b$ , respectively. Then we average the non-Gaussian part of the action, Eq. (9), over the fast fluctuations, i.e. using  $\langle \dots \rangle_{>} \equiv \int \mathcal{D}\phi^>(\dots) e^{-S_{\text{fl}}^>} / \int \mathcal{D}\phi^> e^{-S_{\text{fl}}^>}$ , where  $S_{\text{fl}}^>$  is the fast part of action (15). Applying the identity  $\langle e^{i\phi^>} \rangle_{>} = \exp[-\frac{1}{2}\langle \phi^>^2 \rangle] = b^{-1/2K}$ , we find the non-Gaussian part of the action is renormalized to first order in  $J$  as follows:

$$2J \int d\tau \langle \cos[\phi_{L,R}^<(\tau) + \phi_{L,R}^>(\tau)] \rangle_{>} = b^{1-\frac{1}{2K}} 2J \int d\tau \cos \phi_{L,R}^<(\tau). \quad (16)$$

Differentiating this with respect to  $\ln b$ , we obtained the RG equation (8) given in the main text. Note that since the parts of the action corresponding to the phase drops on the left and on the right are renormalized independently, introducing different tunneling energies for the two barriers will not affect our conclusions. This can also be seen by considering the MF solution in the presence of asymmetric tunneling barriers,  $\alpha_L \neq \alpha_R$ . Following the procedure outlined in the main text, the equations minimizing the asymmetric MF energy are

$$\frac{\Phi_L - \Phi_R}{2} - \phi_+ = \frac{2\alpha_L\alpha_R}{\alpha_L + \alpha_R} \sin \phi_+ \cos \phi_-, \quad (17a)$$

$$\cos \phi_+ \sin \phi_- = \frac{\alpha_L - \alpha_R}{\alpha_L + \alpha_R} \sin \phi_+ \cos \phi_-, \quad (17b)$$

analogous to Eqs. (6) for the symmetric tunneling. A direct comparison of these equations reveals that the symmetric  $\alpha$  of Eq. (6a) is simply replaced by the harmonic average of the asymmetric  $\alpha_L$  and  $\alpha_R$  in Eq. (17a). It can also be seen that Eq. (17b) defines two solutions on  $[0, 2\pi)$  which are shifted away from the solutions,  $\phi_a = 0, \pi$  given in Eq. (6b) for  $J_R = J_L$ , but remain exactly separated by  $\pi$  so that  $\phi_a$  always acts as a label for solutions with  $\pm\alpha_{L(R)}$  in Eq. (17a). Thus, we see that all essential features of the MF solution described in the main text are retained for the case of asymmetric tunneling, with only a simple change of parameters.

### Experimental implementation

The suggested experimental implementation is based on an atom chip, where surface-mounted microfabricated current carrying wires can be employed to form a wide variety of trapping and guiding potentials. The starting point is a moderately elongated initial reservoir trap, in which a BEC of (essentially) three-dimensional nature will be formed. Two parallel Z-shaped wires carrying copropagating currents provide the necessary inhomogeneous fields. Unlike the standard case, the width of the central section of these wires is chosen to vary as a function of position  $x$  along the trap as indicated in Fig. 5. The size of the currents together with the strength of an external homogeneous bias field  $B$  with a direction parallel to the surface plane determines the surface-trap separation  $H$ .

For initial loading,  $H$  is chosen larger than all wire widths and the distance between wires, so that a single simple 3d reservoir trap is formed. Subsequent adiabatic increase in  $B$ , decrease in the wire currents and corresponding reduction of  $H$  will transfer the cloud into two equal 3d reservoirs that are connected through a narrow 1d channel. Additional adjustable currents through thin wires in the direction orthogonal to the channel positioned near its two connection points to the reservoirs are then used to introduce tunable barriers. Raising these barriers and then temporarily introducing a field gradient along  $x$  slightly imbalancing the reservoirs will imprint a differential phase

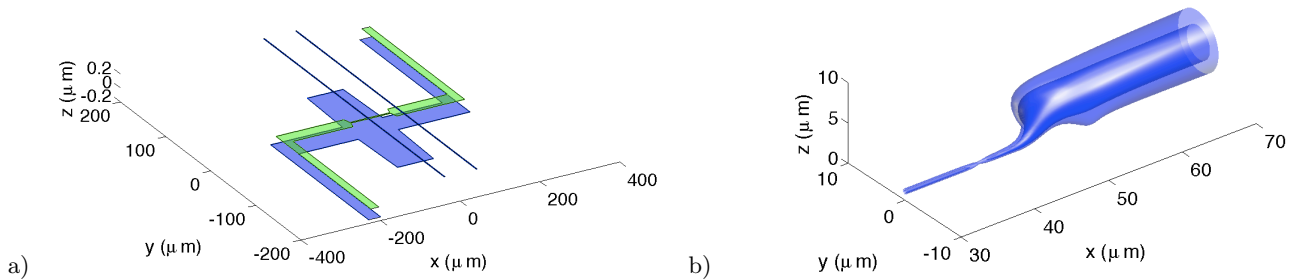


FIG. 5. a) Wire layout in three vertically separated layers on an atom chip. The lower two layers contain Z-shaped wires whose width varies as a function of position as shown. The top layer features two thin wires carrying an independent current that forms barriers of controllable height. b) Typical equipotential surfaces of the trap section where the 3d reservoir is connected to the 1d channel including one of the barriers. Here, the wire currents and external bias field are adjusted to trap the atoms at surface distances of a few micrometers. In contrast, at larger distances of tens to 100 microns a single 3d trap is formed in the same geometry.

between the subclouds trapped in each reservoir. The raised barriers will prevent a chemical potential imbalance between the reservoirs during this preparation procedure.

Information about the supercurrent,  $\mathcal{I} = dE/d\Phi$  can be derived from images taken of the atomic density distribution in the channel at different times throughout the evolution of the system. Absorption images taken after several ms time-of-flight after all confining potentials have been switched off have been demonstrated to reach a sensitivity on the order of 3 atoms/ $\mu\text{m}$  [1]. Due to the strong transverse confinement in the channel, the line density as determined from the integral over the transverse dimensions is essentially unaffected by the time-of-flight. Fluorescence imaging through a sheet of near-resonant light spanned a few mm below the atom chip reaches even single atom sensitivity in the low-density regime [2]. The presence of the cusps would be indicated by jumps in the supercurrent which would provide experimental support for our mean field solution.

As scheme to measure the phase profile predicted in the main text we envision to extend the setup discussed above to an interference experiment. After initial loading of a single reservoir trap, radio-frequency dressing the magnetic trapping potential can be used to vertically (along  $z$ ) split the cloud into two [3]. One cloud is moved close to the surface where the shape of the trapping wires induces the formation of two reservoirs connected by a narrow channel in  $x$ -direction. The other cloud is moved away from the surface, so that it maintains its 3d BEC character with a homogeneous reference phase. At sufficiently large  $z$ -splitting distances, coherence between the clouds will not be maintained, so that the distant BEC provides an independent phase reference. For readout, both clouds are released from the trapping potential, so that they expand (essentially only in the  $yz$ -plane) and overlap. An interference pattern, again detected in absorption or, more sensitively, in fluorescence imaging, will form with a random global phase. However, the phase pattern along  $x$  in the transport channel will be revealed in an inhomogeneous relative phase pattern along  $x$ .

- 
- [1] D. A. Smith, S. Aigner, S. Hofferberth, M. Gring, M. Andersson, S. Wildermuth, P. Krüger, S. Schneider, T. Schumm, and J. Schmiedmayer, *Opt. Express* **19**, 8471 (2011).  
 [2] R. Buecker, A. Perrin, S. Manz, T. Betz, C. Koller, T. Plisson, J. Rottmann, T. Schumm, and J. Schmiedmayer, *New J. Phys.* **11**, 103039 (2009).  
 [3] T. Schumm, S. Hofferberth, L. M. Andersson, S. Wildermuth, S. Groth, I. Bar-Joseph, J. Schmiedmayer, and P. Krüger, *Nat. Phys.* **1**, 5762 (2005).
-